

UCSF

UC San Francisco Previously Published Works

Title

Genetic determinants of co-accessible chromatin regions in activated T cells across humans.

Permalink

<https://escholarship.org/uc/item/8762v2z6>

Journal

Nature genetics, 50(8)

ISSN

1061-4036

Authors

Gate, Rachel E
Cheng, Christine S
Aiden, Aviva P
et al.

Publication Date

2018-08-01

DOI

10.1038/s41588-018-0156-2

Peer reviewed



Published in final edited form as:

Nat Genet. 2018 August ; 50(8): 1140–1150. doi:10.1038/s41588-018-0156-2.

Genetic determinants of co-accessible chromatin regions in activated T cells across humans

Rachel E. Gate^{1,2,21}, Christine S. Cheng^{3,4,21,22}, Aviva P. Aiden^{5,6}, Atsede Siba³, Marcin Tabaka³, Dmytro Lituiev¹, Ido Machol⁵, M. Grace Gordon², Meena Subramaniam^{1,2}, Muhammad Shamim^{5,7}, Kendrick L. Hougén⁸, Ivo Wortman³, Su-Chen Huang⁵, Neva C. Durand⁵, Ting Feng⁹, Philip L. De Jager^{3,10,11}, Howard Y. Chang¹², Erez Lieberman Aiden^{5,7,13,14,15}, Christophe Benoist⁹, Michael A. Beer^{8,16}, Chun J. Ye^{1,17,18,19,22}, and Aviv Regev^{3,20,22}

¹Institute for Human Genetics, University of California, San Francisco, San Francisco, California, USA

²Biological and Medical Informatics Graduate Program, University of California, San Francisco, San Francisco, California, USA

³Klarman Cell Observatory, Broad Institute of MIT and Harvard, Cambridge, Massachusetts, USA

⁴Department of Biology, Boston University, Boston, Massachusetts, USA

⁵Department of Molecular and Human Genetics, the Center for Genome Architecture, Baylor College of Medicine, Houston, Texas, USA

⁶Department of Bioengineering, Rice University, Houston, Texas, USA

⁷Medical Scientist Training Program, Baylor College of Medicine, Houston, Texas, USA

⁸Department of Biomedical Engineering, Johns Hopkins University, Baltimore, Maryland, USA

⁹Division of Immunology, Department of Microbiology and Immunology, Harvard Medical School, Boston, Massachusetts, USA

¹⁰Program in Translational NeuroPsychiatric Genomics, Institute for the Neurosciences, Department of Neurology and Psychiatry, Division of Genetics, Department of Medicine, Brigham and Women's Hospital, Boston, Massachusetts, USA

¹¹Harvard Medical School, Boston, Massachusetts, USA

Users may view, print, copy, and download text and data-mine the content in such documents, for the purposes of academic research, subject always to the full Conditions of use: http://www.nature.com/authors/editorial_policies/license.html#terms

²²Corresponding authors. aregev@broadinstitute.org (A.R.); jimmie.ye@ucsf.edu (C.J.Y.); chcheng@bu.edu (C.S.C.).

²¹These authors contributed equally to this work.

URLs: Partitioned heritability summary statistics, https://data.broadinstitute.org/alkesgroup/sumstats_formatted/.

Author Contributions: A.R., C.J.Y. and C.S.C. conceived this project. C.S.C. and A.S. performed ATAC-seq and RNA-seq assays. I.W. cultured T cells and collected fixed pellet for HiC assay. A.P.A., I.M., M.Sh., S.H., N.C.D., and E.L.A. performed and analyzed the Hi-C dataset. R.E.G., M.T., D.L., M.G.G., and M.Su analyzed the ATAC-seq and RNA-seq datasets. K.L.H and M.A.B. additionally analyzed the ATAC-seq dataset. R.E.G. additionally analyzed the Hi-C dataset. T.F, P.L.D.J, and C.B. provided the patient samples. H.Y.C provided helpful comments and discussion. R.E.G., C.S.C., C.J.Y., and A.R. wrote the manuscript.

Competing Interest: A.R. is an SAB member of ThermoFisher Scientific, Syros Pharmaceuticals and Driver group and a founder of Celsius Therapeutics.

¹²Center for Personal Dynamic Regulomes, Stanford University, Stanford, California, USA

¹³Department of Computer Science, Rice University, Houston, Texas, USA

¹⁴Department of Computational and Applied Mathematics, Rice University, Houston, Texas, USA

¹⁵Center for Theoretical Biological Physics, Rice University, Houston, Texas, USA

¹⁶McKusick-Nathans Institute of Genetic Medicine, Johns Hopkins University, Baltimore, Maryland, USA

¹⁷Institute of Computational Health Sciences, University of California, San Francisco, San Francisco, California, USA

¹⁸Department of Epidemiology and Biostatistics, University of California, San Francisco, San Francisco, California, USA

¹⁹Department of Bioengineering and Therapeutic Sciences, University of California, San Francisco, San Francisco, California, USA

²⁰Howard Hughes Medical Institute, Koch Institute of Integrative Cancer Research, Department of Biology, Massachusetts Institute of Technology, Cambridge, Massachusetts, USA

Abstract

Over 90% of genetic variants associated with complex human traits map to non-coding regions, but little is understood about how they modulate gene regulation in health and disease. One possible mechanism is that genetic variants affect the activity of one or more *cis*-regulatory elements leading to gene expression variation in specific cell types. To identify such cases, we analyzed ATAC-seq and RNA-seq profiles from stimulated primary CD4⁺ T cells in up to 105 healthy donors. We found regions of accessible chromatin (ATAC-peaks) are co-accessible at kilobase and megabase resolution, consistent with the 3D chromatin organization measured by *in situ* Hi-C in T cells. 15% of genetic variants located within ATAC-peaks affected the accessibility of the corresponding peak (ATAC-QTLs). ATAC-QTLs have the largest effects on co-accessible peaks, are associated with gene expression, and are enriched for autoimmune disease variants. Our results provide insights into how natural genetic variants modulate *cis*-regulatory elements, in isolation or in concert, to influence gene expression.

Introduction

The vast majority of disease-associated loci identified through genome-wide association studies (GWAS)^{1–3} are located in non-coding regions of the genome, often distant from the nearest gene⁴. Quantitative trait loci (QTL) studies that associate genetic variants with molecular traits provide a framework for assessing the gene regulatory potential of disease-associated variants. For example, a statistically significant number of GWAS loci are associated with gene expression (expression QTLs – eQTLs) across diverse cell types and states^{5–10}, implicating gene regulation in determining disease risk^{11,12}.

Genetic analysis of variation in chromatin state^{13–17} is a powerful approach for identifying single nucleotide polymorphisms (SNPs) that directly affect *cis*-regulatory activity¹⁸. In

lymphoblastoid cell lines, thousands of SNPs have been associated with DNase I hypersensitivity (measured by DNase-seq)¹⁹ and histone tail modifications (measured by ChIP-seq)^{20–22}. Similarly, SNPs have been associated with variation in DNA methylation and histone tail modifications in resting primary immune cell types (neutrophils, monocytes and CD4⁺/CD45RA⁺ effector memory T cells)¹². Most of the associated SNPs in these studies were also associated with nearby transcript abundance, suggesting the genetic perturbation of *cis*-regulatory activity as a determinant of gene expression variability^{11,12,19,21,23}.

These studies have provided foundational resources for understanding the genetic basis of gene regulation in resting cells, but many disease states are associated with immune cell activation^{24,25}. In particular, dysregulation of T cell homeostasis and activation are known to play a role in autoimmunity^{26,27}, cancer^{28,29} and infectious diseases³⁰, and hundreds of SNPs have been associated with gene expression during T cell activation and polarization^{10,31}. Moreover, because both DNase-seq and ChIP-seq are laborious and require large cell numbers, it remains challenging to apply them to primary human cells at the scale required for genetic association.

Here, we optimized and performed Assay for Transposase Accessible Chromatin sequencing (ATAC-seq) on stimulated CD4⁺ T cells from 105 healthy individuals to characterize the extent of natural variability in chromatin state, identify its genetic basis, and assess its influence on gene expression. We further leveraged the variability between individuals to identify co-accessible chromatin regions and to relate those to genetic variation and 3D genome organization. Our work helps lay the foundation for the critical tasks of annotating *cis*-regulatory elements in primary human T cells and characterizing how genetic variation contribute to variability in gene regulation between individuals.

Results

Changes in T cell chromatin state in response to activation

We used ATAC-seq³² to assay CD4⁺ T cells in two different conditions: either unstimulated (Th), or stimulated *in vitro* using tetrameric antibodies against CD3 and CD28 for 48 hours (Th_{stim}) (Fig. 1a). Aligned reads from six samples (five donors, one pair of donors were replicates) were pooled for each condition, yielding a total of 209 million reads for Th_{stim} and 58 million for Th cells (Methods). Of these five donors, two are of East Asian, two are of African American and one is of European decent (Supplementary Fig. 1). There was a global increase in chromatin accessibility in response to stimulation, with 52,154 chromatin accessible peaks detected in Th_{stim} (average width: 483 bp \pm 344 bp) and 36,487 in Th cells (average width of 520 bp \pm 319 bp) (MACS2, FDR < 0.05, Fig. 1a, b). Downsampling each Th_{stim} sample to the same number of reads as the matching Th sample yielded a similar trend (24,665 Th_{stim} vs. 17,313 Th peaks) suggesting the increased accessibility is not due to differences in sequencing depth. Of the 63,763 peaks identified in at least one condition, 27,446 are similarly accessible between the conditions (shared peaks), 28,017 are more accessible in Th_{stim} cells (Th_{stim}-specific peaks) (FDR < 0.05), and 8,298 are more accessible in Th cells (Th-specific peaks) (FDR < 0.05) (Fig. 1a, b, and Supplementary Table 1).

Peaks of accessible chromatin are associated with distinctive genomic features and enriched for SNPs associated with autoimmune diseases. Compared to Th-specific peaks, Th_{stim}-specific peaks overlap a higher percentage of enhancers defined using H3K27Ac marks¹⁸ in α CD3/ α CD28- (Th₀, 6.9% vs. 2.6%) and phorbol myristate acetate (PMA)-stimulated CD4⁺ T cells (Th_{stim}, 7.2% vs. 3.6%); and a lower percentage of enhancers in regulatory (T_{reg}, 1.4% vs. 4.0%), naïve (T_{naive}, 1.2% vs. 4.9%) and IL17 producing CD4⁺ T cells (Th₁₇, 3.2% vs. 4.6%) (Fig. 1c)¹⁸. Th_{stim}-specific and shared peaks also overlap a higher percentage of SNPs associated with autoimmune diseases, including inflammatory bowel disease (IBD) (32% and 41% vs. 20%) and rheumatoid arthritis (21% and 27% vs. 13%) (Fig. 1d), highlighting the importance of profiling cells under stimulation to identify disease-relevant *cis*-regulatory elements.

Analyzing peaks of accessible chromatin in aggregate provides estimates of the frequencies and single-nucleotide resolution footprints of transcription factor (TF) binding³². Th_{stim}-specific peaks are enriched for genomic locations bound by TFs important for CD4⁺ T cell activation or differentiation, including members of the AP-1 super family (*e.g.*, 36% contain a BATF binding site) and interferon regulatory factors (*e.g.*, 15% contain a IRF4 binding site)^{33–35} (Fig. 2a, b). Th_{stim}-specific peaks overlapping regions bound by both BATF and IRF4 (17.4% of peaks)³⁴ reveal a different footprint compared to those overlapping regions bound by only one of the TFs (Fig. 2b, left). Conversely, shared peaks are enriched for regions bound by CTCF and BORIS (encoded by CTCFL), two transcriptional repressors known to maintain chromatin state independent of cell type and state^{33–35} (Fig. 2a), and their binding footprints are invariant of condition (Fig. 2b, right). ETS1 binding sites overlapping shared, Th_{stim}-, and Th-specific peaks have distinct footprints and binding motifs: we observed the canonical ETS1 motif (5'-CACTTCCTGT-3') in shared peaks, a 3' extended motif (5'-CACTTCCTGTCA-3') in Th-specific peaks, and a T/G to T (5'-CACTTCCTGT-3') substitution at the eighth position in Th_{stim}-specific peaks, consistent with sequence motifs found at distal ETS1 binding sites (Fig. 2c)³⁶. Th-specific peaks are more likely to overlap ETS/RUNX binding sites than shared or Th_{stim}-specific peaks (OR = 2.7 and 3.9; Fisher's exact test, *P*-value < 2.2×10⁻¹⁶ and *P*-value < 2.2×10⁻¹⁶, respectively) (Fig. 2d), which could be due to an enrichment of Th-specific peaks for T_{reg} enhancers known to be bound by the ETS/RUNX complex^{37,38}. An additional 6,102 Th_{stim}-specific (6.6% of intergenic regions) and 4,118 shared peaks (4.5% of intergenic regions) were located in non-coding regions, previously not annotated by H3K27Ac^{18,39}, of which 53.5% and 35.6% overlap known binding sites for TFs in the AP-1 super family and IRF family, respectively. Thus, regions of accessible chromatin overlap both known enhancers and TF binding sites important for polarization-independent activation of T cells, consistent with our stimulation protocol, and in aggregate reveal high-resolution footprints distinguishing condition specific and combinatorial transcription factor binding.

Chromatin co-accessibility at multiple genomic scales

Because Th_{stim}-peaks, including shared and Th_{stim}-specific peaks, better overlap known T cell *cis*-regulatory elements and autoimmune disease loci, we next characterized the inter-individual variability of chromatin accessibility only in stimulated T cells. We optimized the ATAC-seq protocol to profile stimulated CD4⁺ T cells (Supplementary Fig. 2; Methods)

from 105 healthy donors in the ImmVar Consortium¹⁰, all of European descent (Fig. 3a and Supplementary Fig. 1). We obtained a median of 37 million (MAD \pm 13 million) reads per sample, from highly complex libraries with low mitochondrial DNA (mtDNA) contamination (average contamination $< 3\%$, Supplementary Fig. 3). Using a pool of 4.2 billion merged reads from all 105 individuals, we jointly called 167,140 peaks of accessible chromatin (hereafter, ATAC-peaks) (MACS2, FDR < 0.05 , Fig. 3a, b). These included 85.1% of the 52,154 Th_{stim} peaks identified in the initial set of six samples from five individuals with similar enrichment for GWAS loci (Pearson R = 0.65) and enhancer elements (Pearson R = 0.88) (Supplementary Fig. 4).

Leveraging the variability in ATAC-peaks across 105 individuals, we found patterns of co-accessibility (defined as correlation between individual or sets of ATAC-peaks) at multiple genomic scales, recapitulating the 3D chromatin organization, as determined by domain-resolution *in situ* Hi-C⁴⁰ of stimulated CD4⁺ T cells pooled from another five donors (Supplementary Table 2, and Supplementary Fig. 5). At the resolution of 1 Mb bins, we observed significant intra-chromosomal co-accessibility, as measured by correlation of total counts of ATAC-peaks within each bin (Chr1: Fig. 3c, other chromosomes: Supplementary Fig. 6). These pairwise correlations are qualitatively similar to and quantitatively consistent with (Pearson R = 0.66) Hi-C interaction frequencies at the same resolution (Fig. 3d and Supplementary Fig. 6), likely reflecting variability in the signal (regions of accessible chromatin) to noise (regions of inaccessible chromatin) ratio across samples similar to observations in single cells³². At 100 kb resolution, pairwise correlations are also consistent with Hi-C interaction frequencies (Pearson R = 0.52, Supplementary Fig. 7).

We next characterized the co-accessibility between pairs of ATAC-peaks within each 1.5 Mb bin across the genome by linear regression (Fig. 3b, dashed black line, left). After accounting for sources of variation (Supplementary Tables 3 and 4), we found 2,158 pairs of co-accessible peaks enriched for those in close proximity (on average 514 kb apart), encompassing 2% (3,204/167,140) of ATAC-peaks (permutation FDR < 0.05 , Fig. 3e, Supplementary Table 5, and Supplementary Fig. 8). The sequencing coverage of co-accessible peaks is similar to that of all ATAC-peaks (Supplementary Fig. 9a), but they are individually more likely to overlap T_{naïve}, Th_{stim}, and Th₁₇ enhancers (Supplementary Fig. 10) and binding sites for three pioneering factors: NRF, NFY, and STAF (FDR < 0.05 , Supplementary Fig. 11). Pairs of co-accessible peaks were more correlated when both peaks reside in the same contact domain (estimated from Hi-C interactions, Fig. 3f) and 80% consisted of peaks overlapping pairs of *cis*-regulatory annotations (*e.g.* enhancer/enhancer, enhancer/promoter, super enhancer/promoter; Fig. 3g). Finally, co-accessible peaks were enriched in annotated Th_{stim} super-enhancer regions⁴¹ (Fig. 3h, Methods)^{41,42}. These results suggest that chromatin co-accessibility may be determined by the 3D conformation of the genome and may correspond to coordinated regulation of multiple *cis*-regulatory elements, including known T cell enhancers and regions bound by pioneering factors.

Genetic variants associated with chromatin accessibility

We next defined the genetic basis of chromatin accessibility by associating ATAC-peaks with common SNPs (minor allele frequency > 0.05) across the 105 individuals. To maximize

statistical power, we analyzed only the 64,188 SNP-containing ATAC-peaks (Fig. 3b) and found 3,318 that were significantly associated with at least one SNP (RASQUAL⁴³, P -value $< 2.91 \times 10^{-3}$, permutation FDR < 0.05) (Fig. 4a, Supplementary Fig. 12 and Supplementary Table 6). Each best-associated SNP we term a local ATAC quantitative trait locus (*local*-ATAC-QTL) and the corresponding peak a *local*-ATAC-peak (Fig. 3b, middle). We estimate that 15% of the 64,188 peaks are associated with at least one *local*-ATAC-QTL using a method to estimate the proportion of null hypotheses while accounting for incomplete power⁴⁴. Sequencing coverage of *local*-ATAC-peaks was similar to all ATAC-peaks (Supplementary Fig. 9b) and the estimated effects of *local*-ATAC-QTLs are correlated with their effects on H3K27AC ChIP-seq peaks in similar cell types¹² (Supplementary Fig. 13).

Several lines of evidence support a model where *local*-ATAC-QTLs affect accessibility by perturbing *cis*-regulatory elements active in stimulated T cells. First, for the 1,428/3,318 heritable *local*-ATAC-peaks determined by fitting a linear mixed model over SNPs ± 500 kb of each peak⁴⁵ (mean $h^2 = 44\%$, GCTA FDR < 0.05), 81% of the heritability is explained by the corresponding *local*-ATAC-QTLs (Fig. 4b and Supplementary Tables 6 and 7; Methods). This suggests a genetic architecture where a single SNP is responsible for the majority of heritable variation. Second, compared to SNP-containing ATAC-peaks, *local*-ATAC-peaks are preferentially located near transcription start and termination sites (Fig. 4c), are more enriched for T cell enhancers (P -value $< 9.23 \times 10^{-63}$, hypergeometric test; Supplementary Figure 14), and are more enriched for genomic regions bound by TFs involved in T cell development and activation (*e.g.* BATF, AP-1 and IRF) (Supplementary Figure 15). Applying deltaSVM^{46,47} to predict the effects of SNPs on TF binding for 903 ATAC-QTLs located within 300 bp of the middle of the corresponding peaks, we found that almost half (45%) are predicted to strongly disrupt bindings for one of six (BATF, ETS1, IRF, RUNX1, SP1 and CTCF) TF binding sites (Fig. 4d). The effect sizes of *local*-ATAC-QTLs are correlated with SNP motif disruption scores obtained by deltaSVM⁴⁸ (Pearson $R = 0.627$, P -value $< 2.33 \times 10^{-98}$, Fig. 4e; Methods). For *local*-ATAC-peaks that overlap BATF, ETS1 and CTCF binding sites, differential accessibility between genotypes in the core motifs were observed at single nucleotide resolution, even though only 5% of the corresponding *local*-ATAC-QTLs directly alter the core motif sequences. This suggests that the genetic perturbation of TF binding – either directly by disrupting their sites, or more likely indirectly by first disrupting binding by other factors in the same *cis*-regulatory element – may be a major driver for the observed variation in chromatin accessibility across individuals (Fig. 4f and Supplementary Fig. 16). Note that the relation between the accessibility of *local*-ATAC-peaks and 3D chromatin organization is similar to that observed for SNP-containing ATAC-peaks in general (Fig. 4g). Both *local*-ATAC-peaks and SNP-containing ATAC-peaks overlapping BATF and ETS motifs are enriched within Hi-C contact domains, whereas those overlapping CTCF motifs are enriched at the contact domain boundaries (Fig. 4g). These results are consistent with previous reports of CTCF enrichment at contact domain boundaries^{40,49–51}.

Local-ATAC-peaks are more likely to overlap GWAS SNPs from autoimmune diseases than other SNP-containing ATAC-peaks (Supplementary Figure 17), providing a functional context for interpreting disease associations. Even though *local*-ATAC-peaks consist of only ~5% of the SNP-containing ATAC-peaks, they overlap a much larger percentage of the loci

associated with autoimmune diseases including Celiac's disease (28%), Crohn's disease (22%), and rheumatoid arthritis (12%), an 8-fold (hypergeometric P -value $< 4.34 \times 10^{-7}$), 6-fold (hypergeometric P -value $< 8.58 \times 10^{-17}$), and 5-fold (hypergeometric P -value $< 6.18 \times 10^{-8}$) enrichment, respectively. To corroborate this, we performed partitioned heritability analysis to test for enrichment of *local*-ATAC-QTLs in explaining the heritability of 28 common diseases where summary statistics are available. While *local*-ATAC-QTLs are highly enriched for disease associated variants (i.e. Celiac's disease: 6%, enrichment = 51x and Crohn's disease: 7%, enrichment = 63x), the results are not statistically significant after multiple testing correction. However, by relaxing the FDR thresholding for defining *local*-ATAC-QTLs, we found a general trend of increased proportion of heritability explained and statistical significance, and a decrease in enrichment, especially in autoimmune diseases (Fig. 4h; Methods). In fact, all SNP-containing ATAC-peaks (corresponding to FDR < 1) account for a statistically significant proportion of the heritability for all autoimmune diseases ($> 22\%$, Bonferroni-corrected P -value $< 1.3 \times 10^{-2}$, Fig. 4h; Methods). For example, rs17293632 (NC_000015.10:g.67442596C>T) has been associated with Crohn's disease and IBD⁵² and is located in the first intron of *SMAD3*, a gene that encodes for a transcription factor involved in the TGF- β signaling pathway that regulates T cell activation and metabolism⁵³. This SNP disrupts a consensus BATF binding site at a conserved position (deltaSVM=-12.72), and results in decreased chromatin accessibility in individuals that carry the alternate allele (Fig. 4i).

Together, these results suggest that when the accessibility of ATAC-peaks is affected by *local*-ATAC-QTLs residing within peaks, this often involves the disruption of TF binding, even though the SNPs almost always reside outside of the core TF binding site. Moreover, *local*-ATAC-QTLs in stimulated CD4⁺ cells are enriched for autoimmune disease loci, both in the number of overlaps and proportion of heritability explained.

Genetic determinants of chromatin co-accessibility

We next tested if the effect of each *local*-ATAC-QTL could be propagated to co-accessible peaks, for example through 3D chromatin organization, and thus have effects on multiple *cis*-regulatory elements simultaneously. We first estimated the heritability of ATAC-peaks using SNPs ± 500 kb of each peak. As expected, *local*-ATAC-peaks (2,444/3,318 that converged) were more heritable (mean $h^2 = 0.22$) than all ATAC-peaks (Fig. 5a). Co-accessible peaks were also more heritable than all ATAC-peaks, both those containing SNPs (mean $h^2 = 0.44$ vs. mean $h^2 = 0.04$) and those that do not (mean $h^2 = 0.10$ vs. mean $h^2 = 0.04$). Excluding the 3,318 *local*-ATAC-peaks, we identified 382 ATAC-peaks that were associated with a *local*-ATAC-QTL (RASQUAL, P -value $< 1.27 \times 10^{-4}$, permutation FDR < 0.05) located ± 500 kb from the peak. We term each associated SNP a *distal*-ATAC-QTL and each associated peak a *distal*-ATAC-peak (Fig. 2b). Consistent with the heritability analysis, *distal*-ATAC-QTLs imparted the strongest effects on co-accessible peak (Fig. 5b and Supplementary Tables 2, 3).

Co-accessible peaks and co-accessible *distal*-ATAC-peaks are both more likely to overlap Th_{stim} super enhancers than randomly shuffled super enhancers⁴¹. The effect is stronger in co-accessible *distal*-ATAC-peaks (6-fold vs. 4-fold) (Fig. 5c). In an example, rs10882660

(NC_000010.10:g.97517949A>G) is simultaneously a *local*- and *distal*-ATAC-QTL for a pair of co-accessible peaks residing in the 1st and 2nd introns of ectonucleoside triphosphate diphosphohydrolase I (*ENTPDI*) and a Hi-C contact domain (Fig. 5d). *ENTPDI* encodes a protein that is one of the dominant drivers of hydrolysis of ATP and ADP in T_{regs} cells, whose expression can lead to tumor growth in mouse models^{54–57}. These results and example suggest a model where *local*-ATAC-QTLs residing within peaks could also distally affect co-accessible peaks likely reflecting shared genetic effects on pairs of *cis*-regulatory elements.

Linking variation in chromatin state and gene expression

We hypothesized that variants affecting chromatin accessibility (*local*-ATAC-QTLs) would – in some cases – also impact the transcription of the genes controlled through these regulatory regions, and thus provide an important link between variant and target.

To test this hypothesis, we assessed if *local*-ATAC-QTLs are also associated with gene expression in stimulated CD4⁺ T cells, measured by RNA-seq from 95 donors (92 from an aliquot of the same cells with matching ATAC-seq data). After accounting for covariates and principal components for expression heterogeneity (Supplementary Tables 3, 4), we identified 424 genes significantly associated with at least one of 6,903 *local*-ATAC-QTLs located \pm 500 kb from the center of each gene (RASQUAL, P -value $< 1.65 \times 10^{-3}$, permutation FDR < 0.05 , Fig. 6a, and Supplementary Table 8). The 383 best-associated SNPs are eQTLs, and we term the corresponding 424 genes eGenes (Fig. 2b, right). We estimate that 30% of *local*-ATAC-QTLs are also eQTLs (with a procedure to estimate the proportion of null hypotheses; Methods), consistent with previous reports in lymphoblastoid cell lines^{19,21}. Considering all genetic variants located \pm 500 kb from the center of each eGene, we found 191/424 genes to be significantly heritable (GCTA FDR < 0.05), with the eQTL explaining on average 68% of the heritability (Fig. 6b and Supplementary Table 9). The lower estimates of explained heritability than *local*-ATAC-peaks suggests that the genetic control of gene expression may involve more than one SNP and *cis*-regulatory element in some cases.

We next examined the sharing of genetic effects between *local*-ATAC-peaks and eGenes using a bivariate linear mixed model⁴⁵ and mediation analysis⁵⁸. Among the 383 SNPs that are simultaneously associated with chromatin accessibility (as *local*-ATAC-QTLs) and gene expression (as eQTLs), 286 have effect sizes in the same direction (Spearman $\rho = 0.73$) indicative of activating effects, while 138 have effect sizes in the opposite direction indicative of repressive effects (Spearman $\rho = -0.69$) (Fig. 6c). Because of limited sample size, measuring the genetic correlation for individual pairs of *local*-ATAC-peaks and eGenes is likely under powered. However, the distribution of genetic correlations for 161 pairs of *local*-ATAC-peaks and eGenes that converged (inverse variance weighted average of 0.66) was significantly higher than both randomly sampled (inverse variance weighted average of 0.23, Kolmogorov-Smirnov P -value $< 4.32 \times 10^{-10}$) and permuted ATAC-peaks (inverse variance weighted average of 0.07, Kolmogorov-Smirnov P -value $< 1.68 \times 10^{-10}$) (Supplementary Fig. 18 and Supplementary Table 10). This is corroborated by mediation analysis where the genetic effects on 21/424 eGenes were significantly mediated by the

corresponding *local*-ATAC-peaks ($FDR < 0.1$, Fig. 6d) and the high correlation of the mediation effects and the inverse variance weighted genetic correlation (Pearson $R = 0.52$, P -value $< 1.2 \times 10^{-12}$, Supplementary Fig. 19). For example, consider the locus spanning *FADS1* and *FADS2*, genes that encode two fatty acid desaturases (FADS) that regulate inflammation, promote cancer development, and impact dermal and intestinal ulcerations (in *FADS2* knockout mice)^{59–62}. Before conditioning on rs174575 (NC_000011.10:g.61602003C>G), an eQTL for *FADS2* and a *local*-ATAC-QTL for chr11:61,601,708-61,602,451, *FADS2* expression and accessibility of ATAC-peak chr11:61,601,708-61,602,451 are correlated ($R^2 = 0.31$, P -value $< 8.25 \times 10^{-9}$) and after conditioning there is no longer a correlation ($R^2 = 0.08$, P -value $< 6.1 \times 10^{-3}$) (Fig. 6e). Similarly, after conditioning on rs174561 (NC_000011.10:g.61582708T>C), *FADS1* expression is no longer correlated with accessibility of ATAC-peak chr11:61,582,207-61,584,717 (before conditioning: $R^2 = 0.2$, P -value $< 8.74 \times 10^{-6}$; after conditioning: $R^2 = 0.01$, P -value < 0.3) (Fig. 6f). Notably, rs174561 is an eQTL for *FADS1*, a *local*-ATAC-QTL associated with a pair of co-accessible peaks, and has been previously associated with Crohn's disease. It is also in LD with rs174537 (NC_000011.10:g.61552680T>G, $r^2 = 0.82$, $D' = 0.99$), a SNP previously identified as an eQTL in blood^{63,64}. The associated co-accessible peaks span the promoters of *FADS1* and *FADS2* (Fig. 6g, h). These results suggest that 30% of the time, genetic variants associated with chromatin accessibility are also associated with gene expression, and in some cases, such as the *FADS1* and *FADS2* loci previously associated with Crohn's disease, can be directionally linked through mediation analysis.

Discussion

Although variability in gene expression has been extensively characterized, variability in chromatin state has been challenging to study in primary cells. To this end, we analyzed ATAC-seq profiles in primary CD4⁺ T cells from five individuals at rest and in response to stimulation. We found global remodeling of accessible chromatin after stimulation, with a significantly higher number of accessible regions overlapping a large proportion (12 - 28%) of SNPs associated with autoimmune diseases and different T cell enhancer subsets (e.g. T_{regs}, Th₁₇, etc).

Due to these initial observations, we dissected the relationship between genetic variation and variability in chromatin accessibility in a physiologically-relevant system, stimulated CD4⁺ cells. Variation across 105 individuals highlights four inter-related phenomena. **First**, accessible regions co-vary across the genome of an individual (co-accessibility), reflective of the 3D structure of the genome. At individual peak resolution, ~2% of ATAC-peaks are co-accessible, especially if they are within the same Hi-C contact domain, and these are more likely to overlap T cell enhancers, pioneering factors, and “pairs” of regulatory regions, including super-enhancers. These results suggest that co-accessibility between pairs of peaks may be determined by the 3D conformation of the genome and may correspond to coordinated regulation of multiple *cis*-regulatory elements. **Second**, combining genetic variation with variation in individual peak accessibility, we identified *local*-ATAC-QTLs. Even though only a minority (5%) of *local*-ATAC-QTLs directly reside within the core binding sites of TFs, nearly half (45%) are predicted to dramatically disrupt binding at TF

binding sites. Moreover, even though *local*-ATAC-peaks are only 5% of SNP-containing ATAC-peaks, they overlap ~10-30% of the previously reported loci for several common autoimmune diseases and explain 1-7% of the disease heritability. The overwhelming enrichment for autoimmune disease loci among *local*-ATAC-peaks could be the result of both the increased number of features tracking cell state and the propensity for disease-causing variants to perturb *cis*-regulatory elements containing key TFs active in specific cell types or states. **Third**, we found that *local*-ATAC-QTLs can further act *distally* on additional peaks in a 1 Mb window, with the strongest effects on ATAC-peaks that are co-accessible, which substantially increase their mechanistic and functional impact. **Fourth**, considering *local*-ATAC-QTLs in the context of variation in gene expression (by RNA-seq; 92 overlapping individuals), we estimated that 30% of *local*-ATAC-QTLs are also eQTLs, with bivariate and mediation analyses suggesting there may be mechanistic directionality between these functional phenotypes.

In a manner consistent with known modes of transcriptional regulation, our approach for a staged analysis, testing the effects of *local*-ATAC-QTLs on *distal*-ATAC-peaks and gene expression, allowed us to overcome power limitations from the sample size and the technical and biological variability in the assays to detect hundreds of genes associated with *local*-ATAC-QTLs. Despite this, there was limited power for bivariate analysis to quantify the shared genetic effects and establish causality for the observed association to both chromatin state and gene expression. These limitations will likely be overcome in future studies with larger sample sizes and higher sequencing depth.

Our findings, derived from large scale genetic association of quantitative chromatin and gene expression traits in primary human cells implicated in many diseases, provide a molecular framework for how disease-causing variants could alter local chromatin structure to modulate gene expression. With the recent advancement of single cell epigenomic⁶⁵ and transcriptomic^{66,67,68} profiling, it should be possible to more directly detect context-specific genetic effects in a heterogeneous cell population. Future studies that use other disease-relevant primary cells and tissues will help pinpoint causal disease variants and understand the regulatory mechanism underlying common disease.

Materials and Methods

Study subjects and genotyping

Healthy subjects between the ages of 18 to 56 (avg. 29.9) enrolled in the PhenoGenetic study⁸ were recruited from the Greater Boston Area and gave written informed consent for the studies. Individuals were excluded if they had a history of inflammatory disease, autoimmune disease, chronic metabolic disorders or chronic infectious disorders. Genotyping using the Illumina Infinium Human OmniExpress Exome BeadChips (704,808 SNPs are common variants [MAF > 0.01] and 246,229 are part of the exomes; Illumina Inc., San Diego, CA) has been previously described¹⁸. The genotyping success rate was at least 97%. We applied rigorous subject and SNP quality control (QC) that includes: (1) gender misidentification; (2) subject relatedness; (3) Hardy-Weinberg Equilibrium testing; (4) use concordance to infer SNP quality; (5) genotype call rate; (6) heterozygosity outlier; and (7) mismatch detection using SNP overlapping reads from ATAC-seq and RNA-seq. We

excluded 1,987 SNPs with a call rate $< 95\%$, 459 SNPs with Hardy-Weinberg equilibrium P -value $< 10^{-6}$, and 63,781 SNPs with MAF $< 1\%$ from the 704,808 common SNPs (a total of 66,461 SNPs excluded). Principal component analysis of genotypes from all individuals used in the study are shown in Supplementary Figure S6.

We used the IMPUTE2 software (version: 2.3.2) to impute the post-QC genotyped markers from the entire ImmVar cohort ($N = 688$) using reference haplotype panels from the 1000 Genomes Project (The 1000 Genomes Project Consortium Phase III) that contain a total of 37.9 Million SNPs in 2,504 individuals with ancestries from West Africa, East Asia, and Europe. After genotype imputation, we extracted the genotypes for 105 individuals assayed for chromatin accessibility and gene expression. Additional removal of SNPs with MAF < 0.05 in our cohort resulted in 4,558,693 and 4,421,936 common variants tested for chromatin accessibility and gene expression assays, respectively.

Preparation and activation of primary human CD4⁺ T cells

CD4⁺ T cells were isolated and stimulated as previously described¹⁰. Briefly, CD4⁺ T cells were isolated from whole blood by negative selection using RosetteSep human CD4⁺ T cell enrichment cocktail (STEMCELL Technologies Inc., Vancouver, BC) and RosetteSep density medium gradient centrifugation. Isolated CD4⁺ T cells were placed in freezing container at -80°C for overnight, and then moved into a liquid nitrogen tank for long-term storage. On the day of activation, CD4⁺ T cells were thawed in a 37°C water bath, counted and resuspended in RPMI-1640 supplemented with 10% FCS, and plated at 50,000 cells per well in a 96 well round-bottom plate. Cells were either left untreated or stimulated with beads conjugated with anti-CD3 and anti-CD28 antibodies (Dynabeads, Invitrogen #11131D, Life Technologies) at a cell:bead ratio of 1:1 for 48 hours, a time point we previously found to maximize the gene expression response in CD4⁺ T cells. At each time point, cells were further purified by a second step positive selection with CD4⁺ Dynabeads (Invitrogen #11145D, Life Technologies).

ATAC-seq profiling

ATAC-seq profiles were collected for 139 individuals (Supplementary Table 4). We performed ATAC-seq as previously described³², with a modification in the lysis buffer to reduce mitochondrial DNA contamination. 200,000 purified CD4⁺ T cells were lysed with cold lysis buffer (10 mM Tris-HCl, pH 7.4, 10 mM NaCl, 3 mM MgCl₂ and 0.03% tween20). Immediately after lysis, nuclei were spun at 500g for 8 minutes at 4°C . After pelleting the nuclei, we carefully removed the supernatant and resuspended the nuclei with Tn5 transposase reaction mix (25 μl 2X TD buffer, 2.5 μl Tn5 transposase, and 22.5 μl nuclease-free water) (Illumina Inc). The transposition reaction was performed at 37°C for 30 minutes. Immediately after the transposition reaction, DNA was purified using a Qiagen MinElute kit. Libraries were sequenced on an Illumina HiSeq 2500 sequencer to an average read depth of 42 million (± 38 million) per sample (Supplementary Fig. S2), with low mtDNA contamination (0.30 – 5.39%, 1.96% on average), low rates of multiply mapped reads (6.7 – 56%, 19% on average) and a relatively high percentage of usable nuclear reads (60 – 92%, 79% on average).

RNA-seq profiling

RNA-seq profiles were collected for 95 individuals, of which 92 have matching ATAC-seq profiles (Supplementary Table 4). RNA was isolated using Qiagen RNeasy Plus Mini Kit and RNA integrity was quantified by Agilent RNA 6000 Nano Kit using the Agilent Bioanalyzer. Purified RNA were converted to RNA-seq libraries using a previously published protocol⁶⁹, where reverse transcription was carried out based on the SMART template switching method and the resulting cDNA was further tagged and PCR amplified using Nextera XT DNA Sample kit (Illumina) to add the Illumina sequencing adaptors. Samples were sequenced on Illumina HiSeq 2500 to an average depth of 16.9 million reads per sample (+/- 8.7 million).

In situ Hi-C

CD4⁺ T cells were isolated from commercially available fresh blood of healthy individuals (Research Blood Components). CD4⁺ T cells were stimulated for 48 hours with beads conjugated with anti-CD3 and anti-CD28 antibodies. *In situ* Hi-C was performed on the pool of donors as previously described⁴⁰. Cells were crosslinked with 1% formaldehyde for 10 min at room temperature. After nuclei permeabilization, DNA was digested with MboI and digested fragments were labeled using biotinylated d-ATP and ligated. After reverse crosslinking, ligated DNA was purified and sheared to ~400 bp. Biotin labeled DNA fragments were then pulled down with streptavidin beads and prepped for Illumina sequencing⁴⁰. The final libraries were sequenced using Illumina HiSeq and NextSeq to produce ~3.5 billion 100bp paired-end reads.

Alignment of ATAC-seq reads

25bp ATAC-seq reads were aligned to the human genome assembly (hg19) with the Burrows-Wheeler Aligner-MEM (version: 0.7.12)⁷⁰. For each sample, multiply-mapped reads were filtered using Samtools “view”⁷¹ with option “-F 4” and mitochondrial reads were filtered out using BEDtools (function intersectBed)⁷². After filtering, we had a median of 37 million (MAD +/- 13 million) reads per sample.

ATAC-seq peak identification

Filtered ATAC-seq reads from six matched samples (five individuals, of which one individual was repeated) for Th and Th_{stim} cells were merged (separately for Th and Th_{stim} cells) using the Samtools function “merge”⁷¹. Peaks were called on the respective Th and Th_{stim} merged bam files using MACS2 –callpeak (with parameters: –nomodel, –extsize 200, and –shift 100), resulting in 36,486 Th peaks with an average width of 520 bp (+/- 319 bp) and 52,154 Th_{stim} peaks with an average width of 483 bp (+/- 344 bp) (Benjamini-Hochberg FDR < 0.05)⁷³. The Th and Th_{stim} peaks were further merged (using the BEDtools “merge” function), to a total of 63,763 jointly called peaks. BEDtools “coverage”⁷² was used to create a 63,763 (peaks) x 12 (6 samples by 2 conditions) input matrix used for detecting differentially accessible peaks. Differentially accessible peaks between Th and Th_{stim} cells were identified using the DESeq2 R package (version 3.2)⁷⁴, with 8,298 Th-specific peaks (FDR < 0.05, more accessibility in Th cells), 28,017 Th_{stim}-specific peaks (FDR < 0.05, more accessibility in Th_{stim}), and 27,446 shared peaks (FDR > 0.05).

For the co-accessibility and genetic analyses, 4.2 billion filtered ATAC-seq reads from 105 Th_{stim} samples were merged to call 167,140 peaks (FDR < 0.05) using the same parameters as previously described, at an average peak size of 642 bp (+/- 512 bp). Coverage for each peak over all 105 samples was computed.

Percentage of peaks overlapping transcription factor binding motifs

Percentages of MACS2 called peaks overlapping TF binding motifs were computed using the default setting in the Homer suite⁷⁵ function findMotifsGenome.pl (with genome reference hg19, option -size given). For co-accessible peaks and *local*-ATAC-peaks, background overlap percentages were computed using randomly sampled genomic regions preserving the width of each peak to assess the expected TF motif enrichment.

Transcription factor footprinting

Using the Homer suite tool annotatePeaks⁷⁵, and options -m and -mbed, we found all instances of BATF, ISRE, BATF/IRF, ETS1, and CTCF motifs in shared, Th-specific and Th_{stim}-specific peaks. Next, we determined the per-base coverage +/- 1 kb around the center of the motif using BEDtools "coverage", only counting reads that begin at a given location in order to prevent smoothing of the chromatin accessibility signal, and splitting the reads into those that map to the same or opposite strand as the motif to account for biases in ATAC-seq requiring two transposases (i.e. one at a TF binding site and another at a nucleosome accessible region). For each TF footprint, we generated a matrix with the number of rows equal to the number of instances of the motif by 4,000 columns quantifying coverage: +/- 1kb from the same and opposite strand and as the motif. Final TF footprints were derived from median normalized reads.

Outlier analysis and sample mix-up analysis

ATAC-seq samples were further filter if the samples contained a minimum of 8 million QC-passed reads (median of 37 million, MAD +/-13 million) and were highly correlated with other samples (mean Pearson R > 0.68). ATAC-seq and RNA-seq profiles from the 105 individuals were further filtered to identify sample mix-ups. We used the software VerifyBamID⁷⁶ to match each ATAC-seq and RNA-seq sample with the genotyping profile with the highest fIBD score. Samples with designated labels not matching the VerifyBamID predicted genotyping labels were flagged as sample mix-ups. We switched the designated label to the predicted label for cases where the fIBD > 90%. 15 out of the 139 total ATAC-seq samples were re-labeled and four out of the 110 total RNA-seq samples were re-labeled. For the ATAC-seq samples: 18 do not have genotypes, three are outliers, one did not match anyone. For the 110 RNA-seq samples: eight samples do not have genotypes, five are outliers, one did not match anyone. 111 ATAC-seq samples and 96 RNA-seq samples were used in the final analysis after filtering. In the response to activation study, there were five people total, 1 person was repeated for a total of six samples, none were genotyped.

Genetic association analysis of ATAC-peaks

Genetic association analysis was performed on 105 samples of European descent (Supplementary Fig. S6) by running RASQUAL⁴³ on the 167,140 peaks identified in Th_{stim}

cells and 4,558,693 imputed genetic variants, testing variants within a 1 Mb window of each ATAC-peak, and filtering for a minor allele frequency of greater than 5% using uniquely mapped nuclear reads per individual. Sex and ten principal components (Supplementary Table 4) were included as covariates to minimize the effects of confounding factors. Using the RASQUAL “-r” option, 10 permutations were generated for each ATAC-peak. For *local*-ATAC-peak analysis, association statistics for 158,613 peak-SNP pairs where the SNP resides within the peak are compared. For *distal*-ATAC-peak analysis, association statistics for peak-SNP pairs where the SNP does not reside within the peak are compared. In each case, empirical *P*-values and the corresponding false discovery rates were computed using the R qvalue⁴⁴ package to detect a total of 3,318 *local*-ATAC-peaks (FDR < 0.05) and 382 *distal*-ATAC-peaks (FDR < 0.05).

Hi-C data analysis

The sequenced reads were analyzed using the Juicer pipeline⁷⁷. We sequenced 2,940,433,604 Hi-C read pairs in stimulated T cells. Loci were assigned to A and B compartments at 500 kB resolution. Contact domains were annotated using the Arrowhead algorithm with default Juicer parameters at 5kB for stimulated T cells. This yielded a list of 4,008 domains in stimulated T cells at MAPQ > 30. We also ran Arrowhead with these same respective parameters on MAPQ > 0 Hi-C maps, which yielded a list of 4,419 domains in stimulated T cells. The Hi-C maps and feature annotations were visualized using the Juicebox software⁷⁷.

Determination of distance from ATAC-peak to contact domains

We determined the distance from each SNP-containing ATAC-peak to the middle of the closest contact domain. We analyzed the following features: (1) all SNP-containing ATAC-peaks; (2) *local*-ATAC-peaks; and all SNP-containing ATAC-peaks and *local*-ATAC-peaks containing (3) BATF, (4) ETS1, or (5) CTCF motifs. Homer annotatePeaks ‘-mbed’⁷⁵ option was used to identify SNP-containing ATAC-peaks and *local*-ATAC-peaks that contain BATF, ETS1, and CTCF motifs, as previously described. We normalized the distances from each peak to the closest domain by the length of the domain. In order to determine that the distribution of the distance between a given peak and a contact domain is different than the null distribution, we kept the length of each contact domain constant and shuffled the positions of the contact domain. The distances from each peak to the contact domain were binned into 30 bins and divided by the binned distances between a given peak and the shuffled contact domains to determine enrichment at each position.

Co-accessible peak analysis

To identify co-accessible peaks, we computed the correlation between every pair of 167,140 ATAC-peaks within 1.5 Mb of each other using a linear regression model implemented by Matrix eQTL⁷⁸. We first normalized the ATAC-peaks by (1) removing sequencing depth bias using median normalization, (2) standardizing the matrix by subtracting out the mean and dividing by the standard deviation for each peak; and (3) quantile normalizing the matrix⁷⁹. Adjusting for sex and 15 principal components, we used Matrix eQTL to identify 2,158 pairs of co-accessible peaks (1,809 unique ATAC-peaks, FDR < 0.05). We reran the analysis

using 10 permuted datasets generated by shuffling the peak counts for an individual to obtain a distribution of permuted *P*-values. The qvalue package was used to obtain empirical *P*-values and false discovery rates⁴⁴.

RNA-seq analysis

25bp paired end RNA-seq reads were aligned to the hg19 using UCSC transcriptome annotations. Expression levels (expected counts) were determined using RSEM⁷⁹. We applied trimmed mean of M-values normalization method (TMM) to the expected counts using the edgeR package and kept genes that had TMM count > 1 in at least 75% of the samples. For the mapping of eQTLs, we inputted expected counts for filtered genes into RASQUAL⁴³. For the heritability analyses, we used log-transformed TMM counts of filtered genes in order to fit linear mixed models.

Percentage of GWAS loci overlapping

The GREGOR suite⁶³ was used for calculating the percentage of GWAS loci in features of interest: (1) peaks differentially accessible in Th and Th_{stim} cells, (2) co-accessible peaks, (3) SNP-containing peaks, and (4) *local*-ATAC-peaks. GWAS loci in the National Human Genome Research Institute GWAS catalogue as of November 2016 were overlapped. For *local*-ATAC-peaks, peaks were randomly permuted, while retaining the width of each peak to assess the expected GWAS enrichment.

Partitioned heritability analysis

Partitioned heritability analysis was performed using LD Score⁸⁰. Summary statistics for all SNPs for 28 GWAS (Alzheimer, anorexia, autism, bipolar disorder, BMI, celiac, coronary artery disease, crohn's disease, DS, ever smoked fasting glucose, HDL, IBD, LDL, lupus, multiple sclerosis, neuroticism, primary biliary cirrhosis, rheumatoid arthritis, schizophrenia, SWB, triglycerides, type 1 diabetes, type 2 diabetes, ulcerative colitis, years of education 1, and years of education 2) phenotypes were downloaded from the Broad Institute (see URLs). *Local*-ATAC-QTLs were thresholded at FDR < 0.05, FDR < 0.1, FDR < 0.2, FDR < 0.5, and all tested SNPs. Using SNPs at each FDR threshold, annotation files and LD Scores were estimated for all 28 GWAS phenotypes using 'ldsc.py -l2'. Finally, to calculate the partitioned heritability across each phenotype, including our *local*-ATAC-QTLs at each FDR threshold, respectively, 'ldsc.py -h2' was run.

Percentage overlapping T cell annotations

Using the Homer suite annotatePeaks.pl with the -genomeOntology option⁷⁵, we calculated how many of the Th_{stim}-specific peaks, co-accessible peaks, SNP-containing peaks, and *local*-ATAC-peaks fall T cell enhancers¹⁸. For co-accessible peaks, SNP-containing peaks, and *local*-ATAC-peaks peak subsets, background overlap was calculated using randomly sampled genomic regions preserving the width of each peak to assess the expected T cell enrichment.

Proportion in super-enhancer regions

Using the BEDtools “intersect” function, we calculated how many of the co-accessible peaks and co-accessible *local*-ATAC-peaks are also in stimulated Th super-enhancers (as reported in Hinsz et al.⁴¹). Background proportions were computed using randomly sampled genomic regions preserving the length of each super enhancer.

Proportion co-accessible peaks in known regulatory elements

Using the BEDtools “intersect” function⁷², we annotated each peak in our unique pairs of co-accessible peaks as residing in a known Th_{stim} super enhancer (as reported in Hinsz et al.⁴¹), promoter (as reported in Fahr et al.¹⁸), and T cell promoter (as reported in Fahr et al.¹⁸). We determined if each peak in a pair of peaks resided in a promoter and a promoter, promoter and a super enhancer, a promoter and an enhancer, an enhancer and an enhancer, an enhancer and a super enhancer, and a super enhancer and a super enhancer. As background (‘non co-accessible peak’), we used pairs of ATAC-peaks with *P*-value > 0.9, sampled to the same number as co-accessible peaks, and performed the same analysis.

Gkm-SVM and deltaSVM

We ran gkm-SVM^{46,47} on 24,745 300bp ATAC-peaks centered on MACS summits using default parameters and an equal size GC matched negative set, excluding from training any region containing a SNP to be scored by deltaSVM, and repeated with 5 independent negative sets, and averaged the deltaSVM predictions, as previously described⁴⁸. We then calculated deltaSVM for each SNP in a *local*-ATAC-peak, scoring 903 SNPs in 888 loci. We find a Pearson correlation of $R=0.627$ between ATAC-QTL beta and the largest deltaSVM SNP. 777 of the peak *P*-value SNPs had the largest deltaSVM, but 111 flanking SNPs scored more highly than the peak *P*-value SNP and disrupt immune associated TF binding sites. While the gkm-SVM weights fully specify the deltaSVM score, for interpretation we associated the large gkm-SVM weights with the most similar TF PWM from a catalog of JASPAR, Transfac, Uniprobe, and Homer motifs.

Heritability of gene expression and ATAC-peaks

For the univariate analyses, restricted maximum likelihood heritability (h^2) estimates were calculated using GCTA software⁴⁵ with algorithm 1 and no constraints on heritability (*i.e.*, h^2 can be less than 0), while the bivariate analysis was run constrained. For the gene expression heritability analysis, where gene expression was residualized for 12 principal components and sex, and ATAC-peak heritability analysis, where ATAC-peaks were residualized for 10 principal components and sex, we used genotypes ± 500 kb from the transcription start site of the gene and center of each ATAC-peak, respectively. Of the 64,188 SNP-containing ATAC-peaks and 3,318 *local*-ATAC-peaks, 32,317 and 2,444 converged respectively. The bivariate GCTA analysis used genotypes ± 500 kb from the transcription start site of the gene. Randomly sampled ATAC-peaks (non *local*-ATAC-peaks) and permuted ATAC-peaks were plotted as background at the same number of the tested *local*-ATAC-peaks ($N=161$, standard errors < 1).

Mediation of eGenes by *local*-ATAC-peaks

Pairs of *local*-ATAC-peak and eGenes were matched through their shared eQTL. Our normalized ATAC-peak matrix, as previously described (**Methods**), was further adjusted for gender and 10 principal components was used as input *local*-ATAC-peaks. Normalized gene expression matrix, as previously described (**Methods**), was further adjusted for gender and 12 principal components used as input as input for our eGenes. For each eQTL a 92 x three matrix was formatted. Each row in the matrix corresponded to an individual and each column corresponded to (1) eQTL genotype, (2) normalized *local*-ATAC-peak, and (3) normalized eGene. First, we regressed *local*-ATAC-peak ~ eQTL. Second, we regressed eGene ~ eQTL + *local*-ATAC-peak. To test for statistically significant mediation effects, the mediator package⁵⁸ 'mediate' function was called using both regression models as input.

Conditioning on eQTL

For each eQTL, the 92 x three matrix that was previously described (**Methods**) was used as input. To capture the effects of the eQTL, we regressed the eGene ~ *local*-ATAC-peak. To capture the effects after conditioning on the eQTL, we regressed the residuals of eGene ~ eQTL to the *local*-ATAC-peak.

Supplementary Material

Refer to Web version on PubMed Central for supplementary material.

Acknowledgments

We thank the ImmVar participants. We would like to thank Jason Buenrostro for critical reading of the manuscript and advice on ATAC-seq analysis, Jenna Pfiffner and Charles Fulco for initial experimental help with ATAC-seq, Alicia Schep for ATAC-seq nucleosome free caller, Natasha Asinovski and Ho-keun Kwon for help setting up primary T cell cultures and members of the Regev and Ye laboratories for discussions. R.E.G. and C.J.Y. are supported by NIH R01-AR071522 to C.J.Y. M.B. and K.L.H. are supported by NIH HG007348 to M.B., H.Y.C. is supported by NIH grant P50-HG007735, C.S.C is supported by the NIH through a Ruth L. Kirschstein National Research Service Award (F32-DK096822). This work was supported by the Klarman Cell Observatory at the Broad Institute. A.R. is a Howard Hughes Medical Institute Investigator.

Data availability: Raw data are deposited to the Gene Expression Omnibus with accession no. GSE86888.

References

1. McCarthy MI, et al. Genome-wide association studies for complex traits: consensus, uncertainty and challenges. *Nat Rev Genet.* 2008; 9:356–69. [PubMed: 18398418]
2. Visscher PM, Brown MA, McCarthy MI, Yang J. Five years of GWAS discovery. *Am J Hum Genet.* 2012; 90:7–24. [PubMed: 22243964]
3. Hirschhorn JN, Daly MJ. Genome-wide association studies for common diseases and complex traits. *Nat Rev Genet.* 2005; 6:95–108. [PubMed: 15716906]
4. Maurano MT, et al. Systematic localization of common disease-associated variation in regulatory DNA. *Science.* 2012; 337:1190–5. [PubMed: 22955828]
5. Stranger BE, et al. Population genomics of human gene expression. *Nat Genet.* 2007; 39:1217–24. [PubMed: 17873874]
6. Lappalainen T, et al. Transcriptome and genome sequencing uncovers functional variation in humans. *Nature.* 2013; 501:506–11. [PubMed: 24037378]
7. Battle A, et al. Characterizing the genetic basis of transcriptome diversity through RNA-sequencing of 922 individuals. *Genome Res.* 2014; 24:14–24. [PubMed: 24092820]

8. Raj T, et al. Polarization of the effects of autoimmune and neurodegenerative risk alleles in leukocytes. *Science*. 2014; 344:519–23. [PubMed: 24786080]
9. Lee MN, et al. Common genetic variants modulate pathogen-sensing responses in human dendritic cells. *Science*. 2014; 343:1246980. [PubMed: 24604203]
10. Ye CJ, et al. Intersection of population variation and autoimmunity genetics in human T cell activation. *Science*. 2014; 345:1254665. [PubMed: 25214635]
11. Astle WJ, et al. The Allelic Landscape of Human Blood Cell Trait Variation and Links to Common Complex Disease. *Cell*. 2016; 167:1415–1429 e19. [PubMed: 27863252]
12. Chen L, et al. Genetic Drivers of Epigenetic and Transcriptional Variation in Human Immune Cells. *Cell*. 2016; 167:1398–1414 e24. [PubMed: 27863251]
13. Consortium, E.P. An integrated encyclopedia of DNA elements in the human genome. *Nature*. 2012; 489:57–74. [PubMed: 22955616]
14. Gerstein MB, et al. Architecture of the human regulatory network derived from ENCODE data. *Nature*. 2012; 489:91–100. [PubMed: 22955619]
15. Neph S, et al. An expansive human regulatory lexicon encoded in transcription factor footprints. *Nature*. 2012; 489:83–90. [PubMed: 22955618]
16. Thurman RE, et al. The accessible chromatin landscape of the human genome. *Nature*. 2012; 489:75–82. [PubMed: 22955617]
17. Roadmap Epigenomics C, et al. Integrative analysis of 111 reference human epigenomes. *Nature*. 2015; 518:317–30. [PubMed: 25693563]
18. Farh KK, et al. Genetic and epigenetic fine mapping of causal autoimmune disease variants. *Nature*. 2015; 518:337–43. [PubMed: 25363779]
19. Degner JF, et al. DNase I sensitivity QTLs are a major determinant of human expression variation. *Nature*. 2012; 482:390–4. [PubMed: 22307276]
20. Kasowski M, et al. Extensive variation in chromatin states across humans. *Science*. 2013; 342:750–2. [PubMed: 24136358]
21. McVicker G, et al. Identification of genetic variants that affect histone modifications in human cells. *Science*. 2013; 342:747–9. [PubMed: 24136359]
22. Kilpinen H, et al. Coordinated effects of sequence variation on DNA binding, chromatin structure, and transcription. *Science*. 2013; 342:744–7. [PubMed: 24136355]
23. Waszak SM, et al. Population Variation and Genetic Control of Modular Chromatin Architecture in Humans. *Cell*. 2015; 162:1039–50. [PubMed: 26300124]
24. Elinav E, et al. Inflammation-induced cancer: crosstalk between tumours, immune cells and microorganisms. *Nat Rev Cancer*. 2013; 13:759–71. [PubMed: 24154716]
25. Donath MY, Shoelson SE. Type 2 diabetes as an inflammatory disease. *Nat Rev Immunol*. 2011; 11:98–107. [PubMed: 21233852]
26. Ohashi PS. T-cell signalling and autoimmunity: molecular mechanisms of disease. *Nat Rev Immunol*. 2002; 2:427–38. [PubMed: 12093009]
27. Kronenberg M, Rudensky A. Regulation of immunity by self-reactive T cells. *Nature*. 2005; 435:598–604. [PubMed: 15931212]
28. Speiser DE, Ho PC, Verdeil G. Regulatory circuits of T cell function in cancer. *Nat Rev Immunol*. 2016; 16:599–611. [PubMed: 27526640]
29. Restifo NP, Dudley ME, Rosenberg SA. Adoptive immunotherapy for cancer: harnessing the T cell response. *Nat Rev Immunol*. 2012; 12:269–81. [PubMed: 22437939]
30. Belkaid Y, Rouse BT. Natural regulatory T cells in infectious disease. *Nat Immunol*. 2005; 6:353–60. [PubMed: 15785761]
31. Feuerer M, Hill JA, Mathis D, Benoist C. Foxp3+ regulatory T cells: differentiation, specification, subphenotypes. *Nat Immunol*. 2009; 10:689–95. [PubMed: 19536194]
32. Buenrostro JD, Giresi PG, Zaba LC, Chang HY, Greenleaf WJ. Transposition of native chromatin for fast and sensitive epigenomic profiling of open chromatin, DNA-binding proteins and nucleosome position. *Nat Methods*. 2013; 10:1213–8. [PubMed: 24097267]
33. Kurachi M, et al. The transcription factor BATF operates as an essential differentiation checkpoint in early effector CD8+ T cells. *Nat Immunol*. 2014; 15:373–83. [PubMed: 24584090]

34. Li P, et al. BATF-JUN is critical for IRF4-mediated transcription in T cells. *Nature*. 2012; 490:543–6. [PubMed: 22992523]
35. Murphy TL, Tussiwand R, Murphy KM. Specificity through cooperation: BATF-IRF interactions control immune-regulatory networks. *Nat Rev Immunol*. 2013; 13:499–509. [PubMed: 23787991]
36. Cauchy P, et al. Dynamic recruitment of Ets1 to both nucleosome-occupied and -depleted enhancer regions mediates a transcriptional program switch during early T-cell differentiation. *Nucleic Acids Res*. 2016; 44:3567–85. [PubMed: 26673693]
37. Samstein RM, et al. Foxp3 exploits a pre-existent enhancer landscape for regulatory T cell lineage specification. *Cell*. 2012; 151:153–66. [PubMed: 23021222]
38. Hollenhorst PC, et al. DNA specificity determinants associate with distinct transcription factor functions. *PLoS Genet*. 2009; 5:e1000778. [PubMed: 20019798]
39. Chen X, et al. ATAC-seq reveals the accessible genome by transposase-mediated imaging and sequencing. *Nat Methods*. 2016; 13:1013–1020. [PubMed: 27749837]
40. Rao SS, et al. A 3D map of the human genome at kilobase resolution reveals principles of chromatin looping. *Cell*. 2014; 159:1665–80. [PubMed: 25497547]
41. Hnisz D, et al. Super-enhancers in the control of cell identity and disease. *Cell*. 2013; 155:934–47. [PubMed: 24119843]
42. Whyte WA, et al. Master transcription factors and mediator establish super-enhancers at key cell identity genes. *Cell*. 2013; 153:307–19. [PubMed: 23582322]
43. Kumasaka N, Knights AJ, Gaffney DJ. Fine-mapping cellular QTLs with RASQUAL and ATAC-seq. *Nat Genet*. 2016; 48:206–13. [PubMed: 26656845]
44. Storey JD, Tibshirani R. Statistical significance for genomewide studies. *Proc Natl Acad Sci U S A*. 2003; 100:9440–5. [PubMed: 12883005]
45. Yang J, Lee SH, Goddard ME, Visscher PM. GCTA: a tool for genome-wide complex trait analysis. *Am J Hum Genet*. 2011; 88:76–82. [PubMed: 21167468]
46. Ghandi M, Lee D, Mohammad-Noori M, Beer MA. Enhanced regulatory sequence prediction using gapped k-mer features. *PLoS Comput Biol*. 2014; 10:e1003711. [PubMed: 25033408]
47. Ghandi M, M-N M, Ghareghani N, Lee D, Garraway L, Beer MA. gkmSVM, an R package for gapped-kmer SVM. *Bioinformatics*. Apr.2016 19
48. Lee D, et al. A method to predict the impact of regulatory variants from DNA sequence. *Nat Genet*. 2015; 47:955–61. [PubMed: 26075791]
49. Hou C, Zhao H, Tanimoto K, Dean A. CTCF-dependent enhancer-blocking by alternative chromatin loop formation. *Proc Natl Acad Sci U S A*. 2008; 105:20398–403. [PubMed: 19074263]
50. Phillips JE, Corces VG. CTCF: master weaver of the genome. *Cell*. 2009; 137:1194–211. [PubMed: 19563753]
51. Splinter E, et al. CTCF mediates long-range chromatin looping and local histone modification in the beta-globin locus. *Genes Dev*. 2006; 20:2349–54. [PubMed: 16951251]
52. Franke A, et al. Genome-wide meta-analysis increases to 71 the number of confirmed Crohn's disease susceptibility loci. *Nat Genet*. 2010; 42:1118–25. [PubMed: 21102463]
53. Delisle JS, et al. The TGF-beta-Smad3 pathway inhibits CD28-dependent cell growth and proliferation of CD4 T cells. *Genes Immun*. 2013; 14:115–26. [PubMed: 23328844]
54. Enjyoji K, et al. Targeted disruption of cd39/ATP diphosphohydrolase results in disordered hemostasis and thromboregulation. *Nat Med*. 1999; 5:1010–7. [PubMed: 10470077]
55. Deaglio S, et al. Adenosine generation catalyzed by CD39 and CD73 expressed on regulatory T cells mediates immune suppression. *J Exp Med*. 2007; 204:1257–65. [PubMed: 17502665]
56. Plesner L. Ecto-ATPases: identities and functions. *Int Rev Cytol*. 1995; 158:141–214. [PubMed: 7721538]
57. Sun X, et al. CD39/ENTPD1 expression by CD4+Foxp3+ regulatory T cells promotes hepatic metastatic tumor growth in mice. *Gastroenterology*. 2010; 139:1030–40. [PubMed: 20546740]
58. Hicks R, Tingley D. Causal Mediation Analysis. *Stata Journal*. 2011; 4
59. Fan YY, et al. Characterization of an arachidonic acid-deficient (Fads1 knockout) mouse model. *J Lipid Res*. 2012; 53:1287–95. [PubMed: 22534642]

60. Barrie A, et al. Prostaglandin E2 and IL-23 plus IL-1beta differentially regulate the Th1/Th17 immune response of human CD161(+) CD4(+) memory T cells. *Clin Transl Sci.* 2011; 4:268–73. [PubMed: 21884514]
61. Sakata D, Yao C, Narumiya S. Prostaglandin E2, an immunoactivator. *J Pharmacol Sci.* 2010; 112:1–5. [PubMed: 20051652]
62. Stroud CK, et al. Disruption of FADS2 gene in mice impairs male reproduction and causes dermal and intestinal ulceration. *J Lipid Res.* 2009; 50:1870–80. [PubMed: 19351970]
63. Schmidt EM, et al. GREGOR: evaluating global enrichment of trait-associated variants in epigenomic features using a systematic, data-driven approach. *Bioinformatics.* 2015; 31:2601–6. [PubMed: 25886982]
64. Marigorta UM, et al. Transcriptional risk scores link GWAS to eQTLs and predict complications in Crohn's disease. *Nat Genet.* 2017; 49:1517–1521. [PubMed: 28805827]
65. Buenrostro JD, et al. Single-cell chromatin accessibility reveals principles of regulatory variation. *Nature.* 2015; 523:486–90. [PubMed: 26083756]
66. Klein AM, et al. Droplet barcoding for single-cell transcriptomics applied to embryonic stem cells. *Cell.* 2015; 161:1187–201. [PubMed: 26000487]
67. Macosko EZ, et al. Highly Parallel Genome-wide Expression Profiling of Individual Cells Using Nanoliter Droplets. *Cell.* 2015; 161:1202–14. [PubMed: 26000488]
68. Kang HM, et al. Multiplexed droplet single-cell RNA-sequencing using natural genetic variation. *Nat Biotechnol.* 2018; 36:89–94. [PubMed: 29227470]
69. Satija R, Farrell JA, Gennert D, Schier AF, Regev A. Spatial reconstruction of single-cell gene expression data. *Nat Biotechnol.* 2015; 33:495–502. [PubMed: 25867923]
70. Li H, Durbin R. Fast and accurate long-read alignment with Burrows-Wheeler transform. *Bioinformatics.* 2010; 26:589–95. [PubMed: 20080505]
71. Li H, et al. The Sequence Alignment/Map format and SAMtools. *Bioinformatics.* 2009; 25:2078–9. [PubMed: 19505943]
72. Quinlan AR, Hall IM. BEDTools: a flexible suite of utilities for comparing genomic features. *Bioinformatics.* 2010; 26:841–2. [PubMed: 20110278]
73. Zhang Y, et al. Model-based analysis of ChIP-Seq (MACS). *Genome Biol.* 2008; 9:R137. [PubMed: 18798982]
74. Love MI, Huber W, Anders S. Moderated estimation of fold change and dispersion for RNA-seq data with DESeq2. *Genome Biol.* 2014; 15:550. [PubMed: 25516281]
75. Heinz S, et al. Simple combinations of lineage-determining transcription factors prime cis-regulatory elements required for macrophage and B cell identities. *Mol Cell.* 2010; 38:576–89. [PubMed: 20513432]
76. Jun G, et al. Detecting and estimating contamination of human DNA samples in sequencing and array-based genotype data. *Am J Hum Genet.* 2012; 91:839–48. [PubMed: 23103226]
77. Durand NC, et al. Juicer Provides a One-Click System for Analyzing Loop-Resolution Hi-C Experiments. *Cell Syst.* 2016; 3:95–8. [PubMed: 27467249]
78. Shabalin AA. Matrix eQTL: ultra fast eQTL analysis via large matrix operations. *Bioinformatics.* 2012; 28:1353–8. [PubMed: 22492648]
79. Li B, Dewey CN. RSEM: accurate transcript quantification from RNA-Seq data with or without a reference genome. *BMC Bioinformatics.* 2011; 12:323. [PubMed: 21816040]
80. Finucane HK, et al. Partitioning heritability by functional annotation using genome-wide association summary statistics. *Nat Genet.* 2015; 47:1228–35. [PubMed: 26414678]

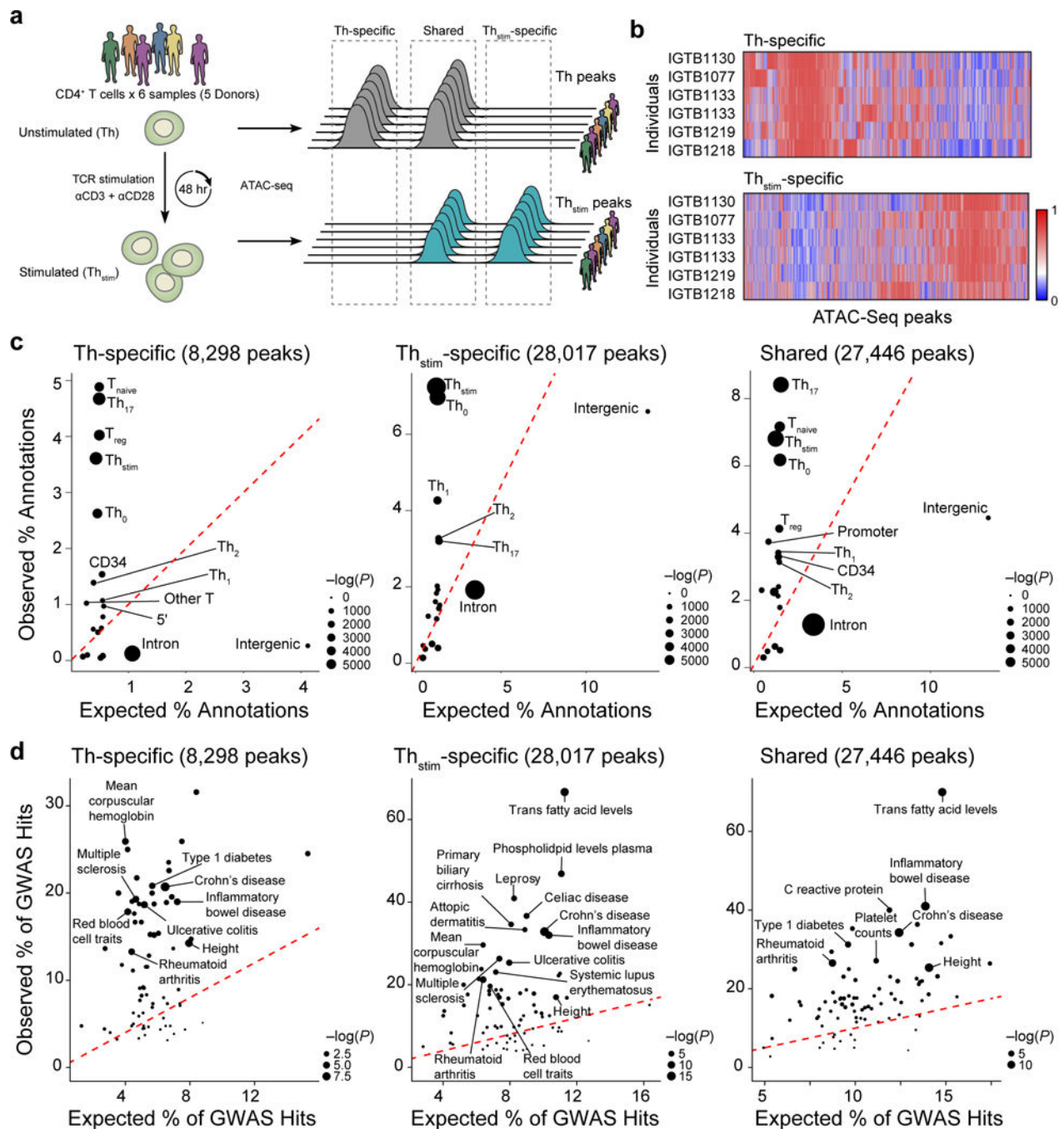


Figure 1. Changes in chromatin state in human T cell activation

(a) Experimental overview (left) and schematic of nomenclature (right). (b) Differential chromatin accessibility. Regions of open chromatin (columns) in six samples (rows) before (top, Th-specific) and 48hr after (bottom, Th_{stim}-specific) activation of primary T cells with anti-CD3/CD28 antibodies. (c) Overlap with previously annotated T cell enhancers. For each annotation, expected (x-axis) vs. observed (y-axis) percentages of annotated features overlapping Th-specific (left), Th_{stim}-specific (center) and shared peaks (right). (d) Overlap with GWAS variants. For each phenotype or disease, expected (x-axis) vs. observed (y-axis)

percentages of GWAS loci overlapping Th-specific (left), Th_{stim}-specific (center), or shared (right) peaks.

Author Manuscript

Author Manuscript

Author Manuscript

Author Manuscript

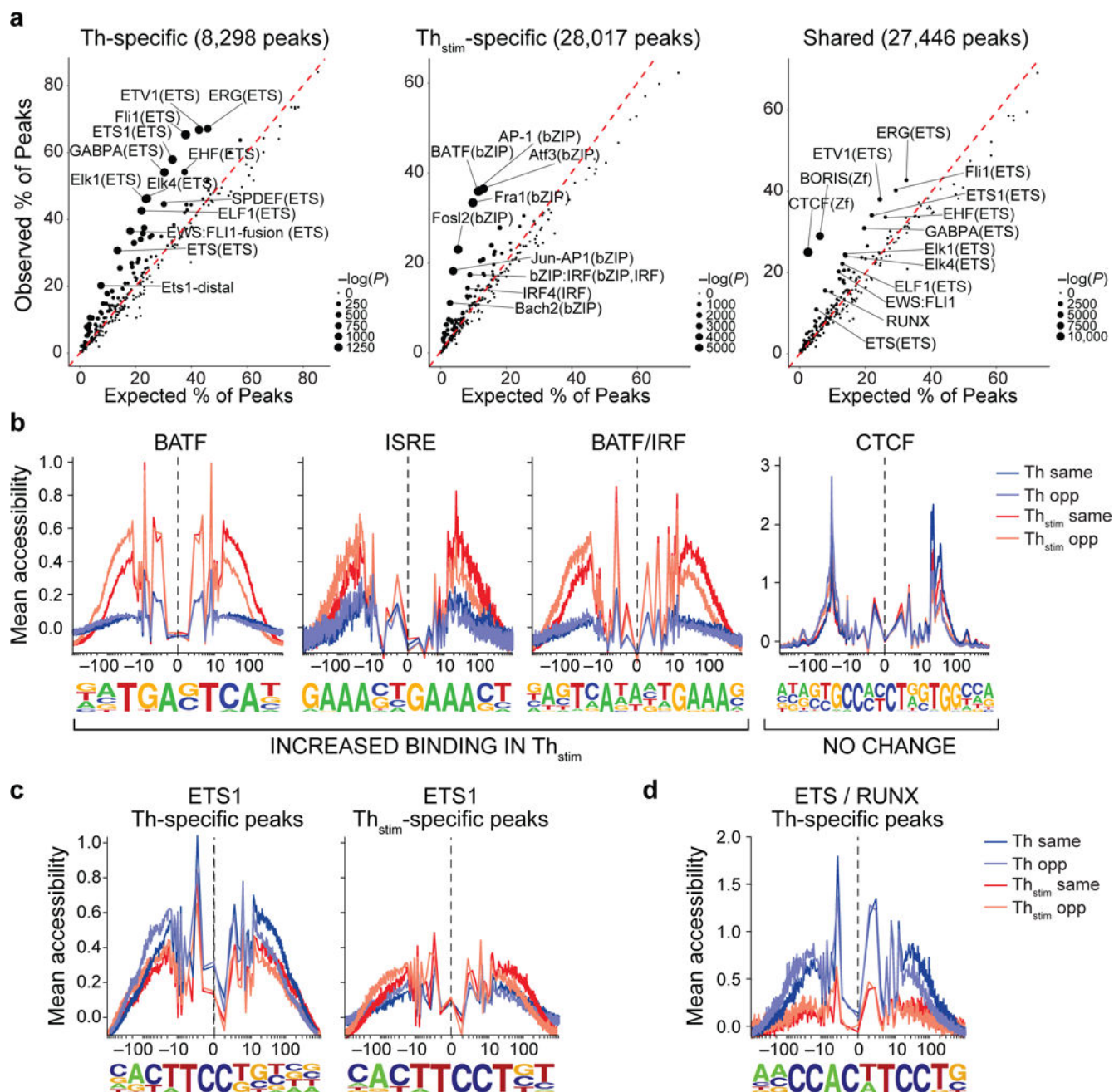


Figure 2. Changes in transcription factor enrichment in response to T cell activation
(a) Transcription factor motif enrichment. Expected (x-axis) vs. observed (y-axis) percentages of Th-specific (left), Th_{stim}-specific (center), or shared (right) peaks overlapping each TF binding site annotation. **(b-d)** TF footprinting. For each TF motif (as defined in ENCODE⁶³), nucleotide resolution average chromatin accessibility (y-axis) in Th (purple) or Th_{stim} (red) cells along the TF binding site (x-axis; log(bp from center of each TF motif)). Aggregated locations are defined as **(b)** Th_{stim}-specific peaks overlapping BATF, ISRE, and BATF/IRF motifs (three left panels) and shared peaks overlapping CTCF binding sites (right

panel), (c) Th-specific (left) and Th_{stim}-specific (right) peaks overlapping ETS1 binding sites, and (d) Th-specific peaks overlapping ETS1/RUNX combinatorial binding sites.

Author Manuscript

Author Manuscript

Author Manuscript

Author Manuscript

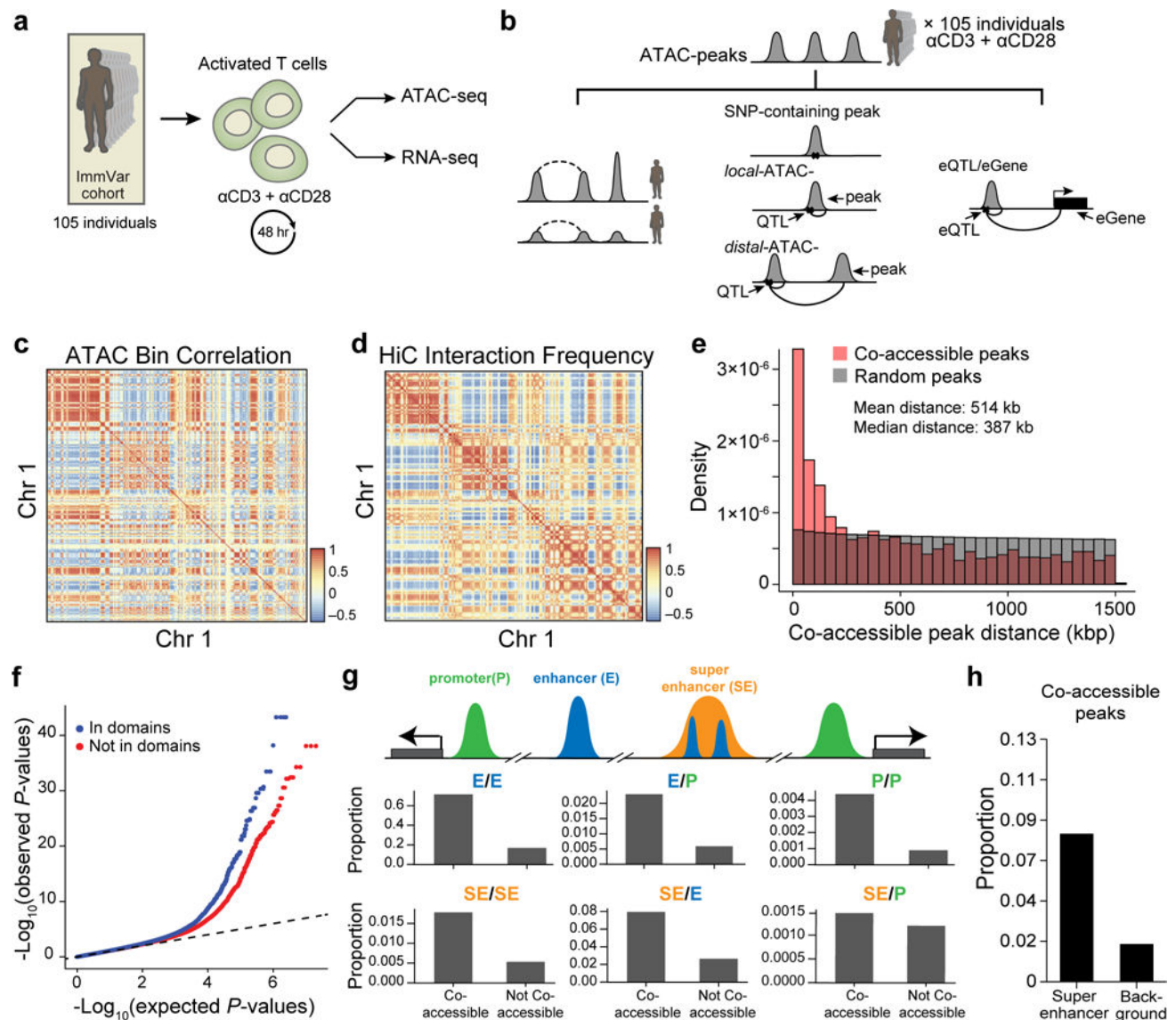


Figure 3. Inter-individual chromatin co-accessibility

(a) Overview of T cell activation for 105 ATAC-seq and 95 RNA-seq samples. (b) Schematic of nomenclature for co-accessible peaks, SNP-containing peaks, *local*-ATAC-QTLs, *distal*-ATAC-QTLs, and eQTLs. Dashed lines denote a correlation between co-accessible peaks and solid lines denote a genetic association. (c) Megabase scale correlation of chromatin accessibility across 105 individuals. Heat map shows the pairwise Pearson correlation of chromatin accessibility between 1 Mb bins (row, column) for Chr 1. (d) Pearson correlation of Hi-C interactions at 1 Mb resolution for Chr 1. (e) Histogram of distances between significantly co-accessible peaks (pink) and random permuted peaks (grey). (f) Co-accessible peaks overlap with Hi-C domains. Q-Q plot of linear regression P -values for pairs of peaks residing in (blue) or out (red) of the same Hi-C domain. (g) Pairs of co-accessible peaks overlapping with multiple *cis*-regulatory regions. A cartoon depiction (top) of co-accessible peaks in promoters (green), enhancers (blue), and super enhancers (orange). Proportion (y-axis) of pairs of co-accessible peaks and non-co-accessible peaks

overlapping pairs of annotated *cis*-regulatory elements (right). **(h)** Proportion of co-accessible peaks overlapping super-enhancers or randomly shuffled background.

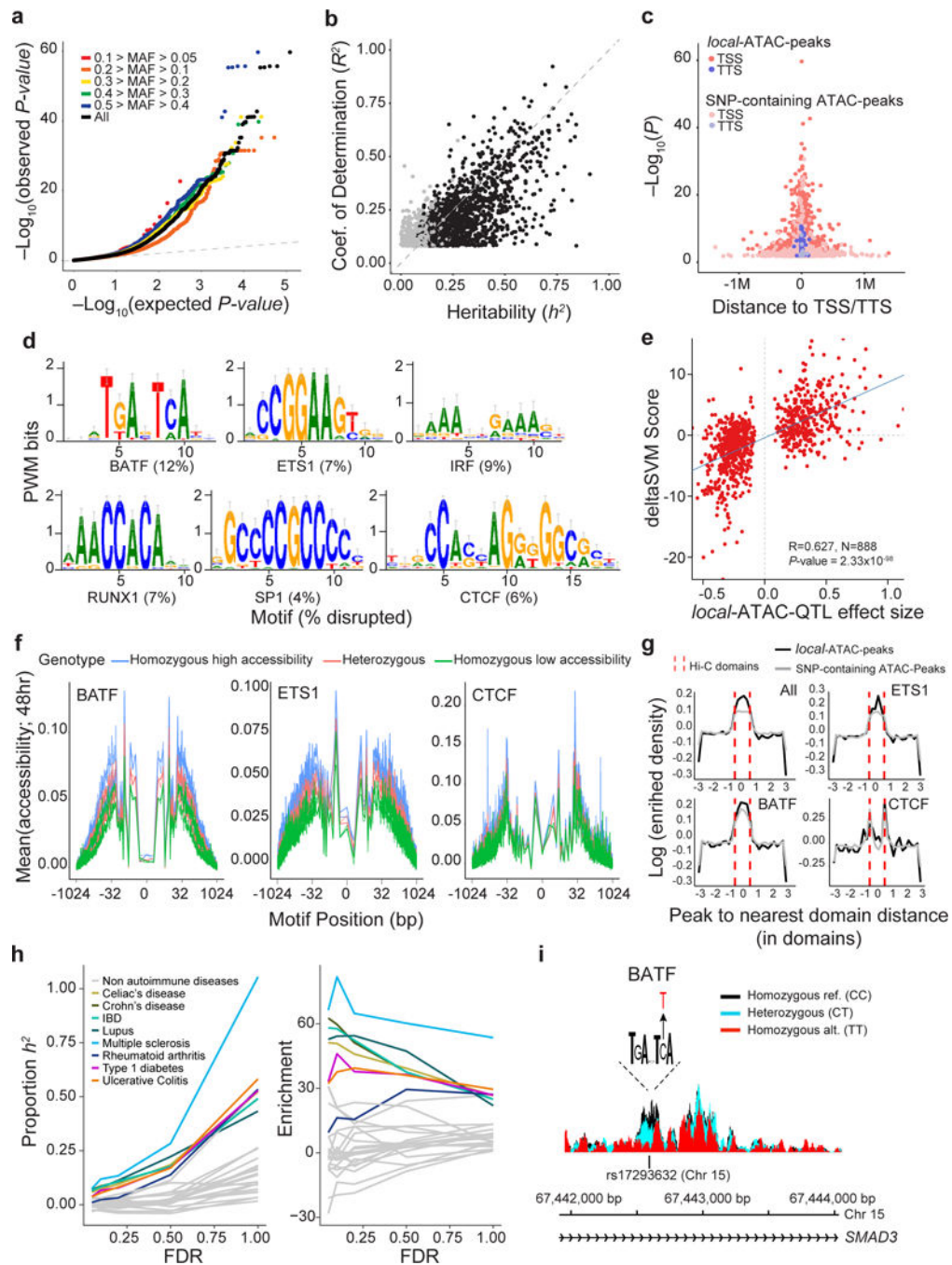


Figure 4. Genetic variants that affect chromatin states in human T cell activation

(a) Q-Q plot of linear regression P -values for all *local*-ATAC-QTLs (black) and *local*-ATAC-QTLs binned by minor allele frequency: 0.1 > MAF > 0.05 (red), 0.2 > MAF > 0.1 (orange), 0.3 > MAF > 0.2 (yellow), 0.4 > MAF > 0.3 (green), 0.5 > MAF > 0.4 (blue), and MAF > 0.05 (black). (b) Heritability of chromatin accessibility. For each of 1,428 *local*-ATAC-peaks, coefficient of determination (R^2) of the best associated *local*-ATAC-QTL (y-axis) vs. *cis* heritability (h^2) estimated based on all genotypes \pm 500 kb of each peak (x-axis). Black points: significantly heritable peaks (FDR < 0.05). (c) Enrichment of *local*-ATAC-peaks in

TSS and TTS. 3,318 *local*-ATAC-peaks (dark pink and purple) vs. 3,318 randomly sampled SNP-containing ATAC-peaks (light pink and purple). **(d-f)** Disruption of TF binding sites by *local*-ATAC-QTLs. **(d)** Unsupervised TF binding site analysis of *local*-ATAC-peaks. Motifs for six TFs associated with most of the large gkmSVM weights, and the percentage of the overall disruption (% , bottom) explained by *local*-ATAC-QTLs. **(e)** Correlation of effect sizes of *local*-ATAC-QTLs (x-axis) vs. deltaSVM scores (y-axis). **(f)** Allele specificity of *local*-ATAC-QTLs. For BATF, ETS1 and CTCF motifs (as identified in ENCODE⁶³), aggregated plots of mean chromatin accessibility (y-axis) of *local*-ATAC-peaks along the TF binding site (x-axis; log(bp from center of the TF motif)) for samples heterozygous (pink), homozygous for the high (blue) or low (green) *local*-ATAC-QTL alleles **(g)** Relation between contact domains and SNP-containing ATAC-peaks or *local*-ATAC-peaks. For ATAC-peaks or *local*-ATAC-peaks overlapping ETS1, CTCF, or BATF binding sites, enrichment density (y-axis) vs. distance (number of domains) of peak to nearest domain (x-axis). Hi-C contact domain boundaries are indicated (dotted red lines). **(h)** Partitioned heritability estimates. The proportion of the heritability for 28 diseases explained (proportion: left, y-axis; enrichment: right, y-axis) captured by *local*-ATAC-QTLs called at different FDR thresholds (x-axis). **(i)** Effects of *local*-ATAC-QTL rs17293632 on the accessibility of the corresponding BATF containing *local*-ATAC-peak on chromosome 15. ATAC-seq profiles were aggregated per rs17293632 genotypes (black: homozygous major allele, light blue: heterozygous, red: homozygous minor allele).

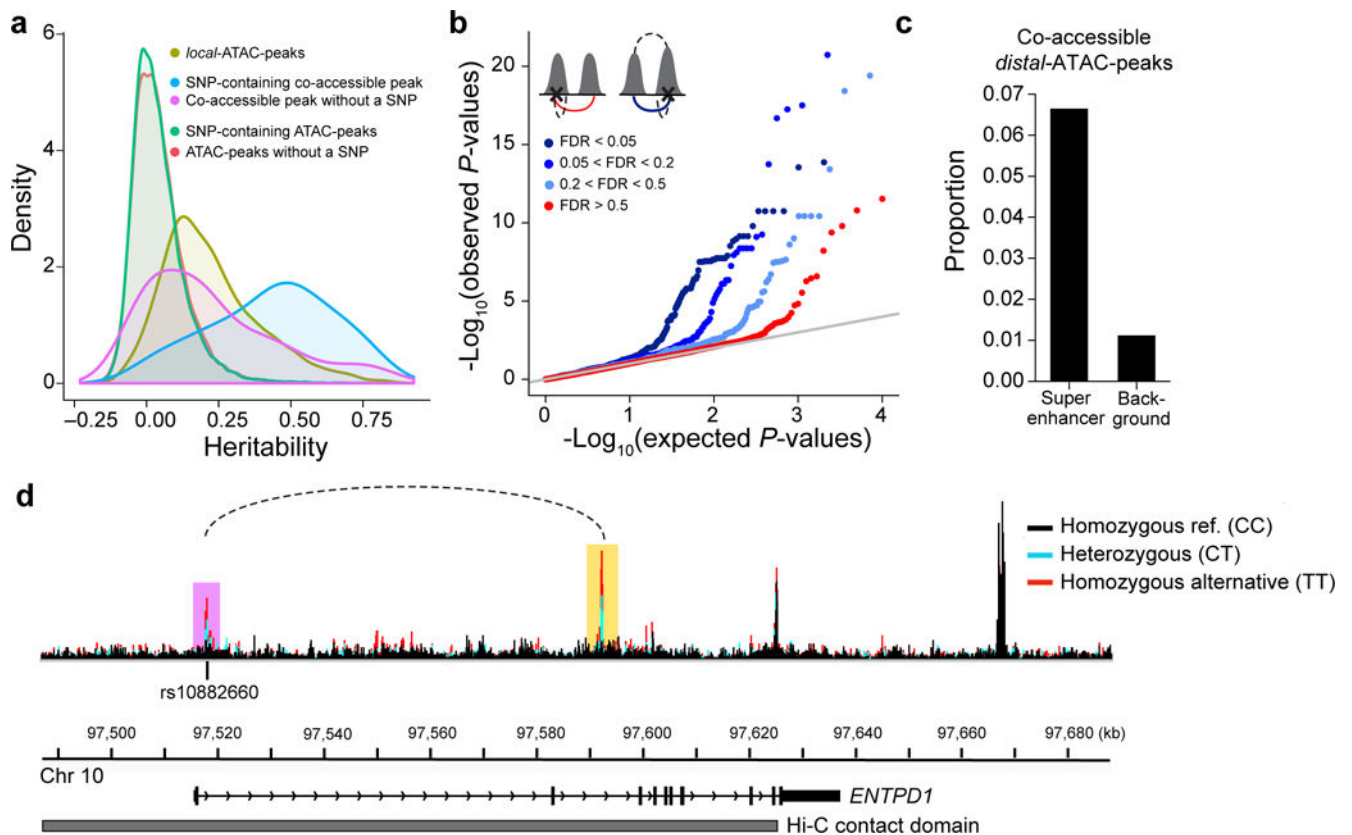


Figure 5. Genetic determinants of co-accessible peaks

(a) Distribution of the heritability explained by SNPs ± 500 kb of ATAC-peaks. *Local*-ATAC-peaks (olive). SNP-containing co-accessible peaks (blue). Co-accessible peaks without a SNP (purple). SNP-containing ATAC-peaks (green). ATAC-peaks without a SNP (red). (b) Q-Q plots of the linear regression P -values of *distal*-ATAC-peaks that are single peaks (red: co-accessibility FDR > 0.5), or co-accessible peaks called at various significance cutoffs (light blue: $0.2 < \text{FDR} < 0.5$, medium blue: $0.05 < \text{FDR} < 0.2$, dark blue: FDR < 0.05). The cartoons (upper left corner) depict the *distal*-ATAC-QTL association for single peaks (left cartoon; red line is the association plotted) and *distal*-ATAC-QTL association for co-accessible peaks (right cartoon; blue line is the association plotted; upper dashed line is the co-accessible peak at various significance cutoffs). (c) Proportion of co-accessible *distal*-ATAC-peaks overlapping super-enhancers or randomly shuffled background. (d) An example of a genetic variant (rs10882660) residing in the first intron in *ENTPD1*, associated *locally* (in purple) and *distally* (in yellow) to ATAC-peaks. The *local* and *distal*-ATAC-peaks are co-accessible (dotted line) and reside in a Hi-C contact domain (grey). ATAC-seq profiles were aggregated for individuals of different rs10882660 genotypes (black: homozygous major allele, light blue: heterozygous, red: homozygous minor allele).

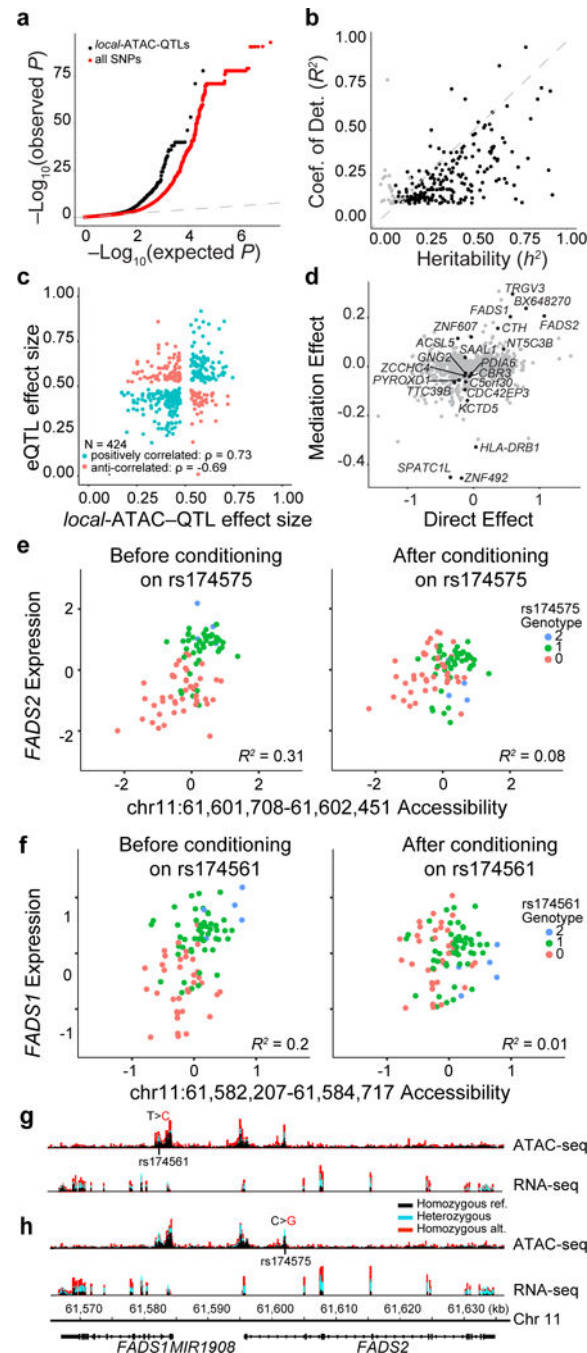


Figure 6. Association of chromatin accessibility and gene expression

(a) eQTLs. Q-Q plot of associations between *local*-ATAC-QTLs (black) or all SNPs (red) and expression of genes \pm 500kb. (b) Heritability of gene expression. For each of 191 eGenes, coefficient of determination (R^2) of the best associated eQTL (y-axis) vs. heritability (h^2) of all variants \pm 500 kb of each gene (x-axis). Black points: significantly heritable peaks (FDR < 0.05). (c) Correlation of effect sizes between *local*-ATAC-QTLs (x-axis) and eQTLs (y-axis). (d) Mediation of eGenes. Average causal mediation effect estimates (y-axis) and average direct effect estimates (x-axis) for *local*-ATAC-peaks

(mediator) and eGenes (outcome variable) sharing a SNP (instrument variable). $FDR < 0.1$ *local*-ATAC-peaks are colored in black. **(e,f)** Examples of gene expression conditioned on chromatin accessibility. **(e)** *FADS2* expression (y-axis) vs. chromatin accessibility at chr11:61,601,708-61,602,451 (x-axis) before (left) and after (right) conditioning on rs174575. **(f)** *FADS1* expression (y-axis) vs. chromatin accessibility at chr11:61,582,207-61,584,717 (x-axis) before (left) and after (right) conditioning, colored by rs174561 genotypes. **(g,h)** ATAC-seq (top) and RNA-seq (bottom) profiles were aggregated for individuals of different **(g)** rs174561 and **(h)** rs174575 genotypes (black: homozygous major allele, light blue: heterozygous, red: homozygous minor allele).